III International Conference on Particle-based Methods – Fundamentals and Applications
PARTICLES 2013
M. Bischoff, E. Oñate, D.R.J. Owen, E. Ramm & P. Wriggers (Eds)

# EXPERIMENTAL AND DISCRETE ELEMENT MODELLING OF COHESIVE IRON ORE FINES

**J.P. MORRISSEY[1], J.Y. OOI[1], J.F. CHEN[2], K. TANO[3] AND G. HORRIGMOE[4]**

[1] Institute for Infrastructure and Environment,
School of Engineering, The University of Edinburgh, EH9 3JL, Scotland, U.K
E-mail: j.ooi@ed.ac.uk

[2] School of Planning, Architecture and Civil Engineering, Queen's University Belfast,
Belfast, Antrim, BT9 5AG, Northern Ireland, UK

[3] LKAB, Malmberget SE-983 81, Sweden

[4] Sweco Norge, Narvik NO-8514, Norway

**Key words:** Granular materials, DEM, discrete element method, flow function, uniaxial test, iron ore fines, cohesive solid.

**Abstract.** In this study, the behaviour of iron ore fines with varying levels of adhesion was investigated using a confined compression test and a uniaxial test. The uniaxial test was conducted using the semi-automated uniaxial EPT tester in which the cohesive strength of a bulk solid is evaluated from an unconfined compression test following a period of consolidation to a pre-defined vertical stress. The iron ore fines were also tested by measuring both the vertical and circumferential strains on the cylindrical container walls under vertical loading in a separate confined compression tester – the $K_0$ tester, to determine the lateral pressure ratio.

Discrete Element Method simulations of both experiments were carried out and the predictions were compared with the experimental observations. A recently developed DEM contact model for cohesive solids, an Elasto-Plastic Adhesive model, was used. This particle contact model uses hysteretic non-linear loading and unloading paths and an adhesion parameter which is a function of the maximum contact overlap. The model parameters for the simulations are phenomenologically based to reproduce the key bulk characteristics exhibited by the solid.

The simulation results show a good agreement in capturing the stress history dependent behaviour depicted by the flow function of the cohesive iron ore fines while also providing a reasonably good match for the lateral pressure ratio observed during the confined compression $K_0$ tests. This demonstrates the potential for the DEM model to be used in the simulation of bulk handling applications.

## 1 INTRODUCTION

Bulk handling of powders and granular solids is common in many industries and often gives rise to handling difficulties especially when the material exhibits complex cohesive behaviour. For example, high storage stresses in a silo can lead to high cohesive strength of the stored solid, which may in turn cause blockages such as ratholing or arching near the outlet during discharge. The cohesive strength of a bulk material depends on the consolidation stress it has experienced. As a result, the stress history in the material leading up to a handling scenario needs to be considered when evaluating its handling behaviour.

The discrete element method (DEM) has been extensively used to simulate the behaviour of granular materials. For cohesive solids, it is crucial that the stress history dependent behaviour is adequately captured. A number of contact models are available in several commercial DEM packages to simulate cohesive granular materials. These include the JKR model [1] and capillary force models [2], [3], [4], [5]. However, DEM simulations with these models may not capture the stress history dependency behaviour observed in bulk solids. A recently developed DEM contact model for cohesive solids [6], [7] was used to assess whether the DEM model can capture the confined compression and uniaxial loading behaviour of iron ore fines. The elasto-plastic adhesive model are phenomenologically based, with the target of capturing the key bulk characteristics exhibited by the solid.

## 2 EXPERIMENTAL BEHAVIOUR OF COHESIVE GRANULAR MATERIALS

The flowability of bulk solids, particularly fine grained ones, is greatly affected by the adhesive forces that act between the particles. In moist bulk solids, the capillary forces and solid bridging tend to become the dominant adhesive forces, while van der Waals forces become less influential as particle size increases past several microns. In the case of the iron ore fines which are relatively large, dense particles, it is expected that the effect of moisture will be most significant. The flowability of bulk solids is usually measured using the flow function, which is the relationship between the unconfined yield strength ($\sigma_u$) and the consolidation stress ($\sigma_1$). The flowability characteristics were measured as described below.

### 2.1 Test Material

The iron ore fines in this study are the < 6.3 mm fractions that are broken from the main iron ore pellets during handling or storage. The iron ore fines are from LKAB and both Direct Reduction (KPRS) and Blast Furnace (KPBO) pellet fines have been studied. The material had a quoted bulk density of 2300 kg/m$^3$ and solid density of 3700 kg/m$^3$. For this study only the finer fractions passing a 1.18 mm sieve are tested in the Edinburgh Powder Tester while the full size range of particles (< 6.3 mm) was used for the larger scale confined compression test. The behaviour of the iron ore fines is expected to be affected by both the moisture content and the temperature of the sample. Only the effect of moisture content is investigated here. The fines were evaluated at eight different moisture content levels for the confined compression tests: ranging from dry (< 0.2%) to 10% and at 5 different levels for the unconfined uniaxial test: 1%, 2%, 3%, 4% and 6%. Dry iron ore fines are not included as they did not display any cohesive strength up to a consolidation stress of 80 kPa. The moisture content percentage MC (on a dry basis) was measured by drying a sample in an oven at 105°C for 24 hours.

## 2.2 Edinburgh Powder Tester

Both the confined and unconfined responses of the iron ore fines were measured using the Edinburgh Powder Tester (EPT). The EPT is a semi-automated uniaxial tester (Fig. 1), in which the unconfined compressive strength ($\sigma_u$) of a bulk solid is evaluated from an unconfined compression test, following a period of consolidation to a pre-defined stress level ($\sigma_1$). After the removal of the consolidation stress, the confining tube is slid off carefully and a vertical force is applied to the sample through the top platen until failure of the sample. The EPT also allows for the evaluation of the bulk compressibility of a material by measuring the height of the sample at incremental consolidation loads during a confined compression test. As the load is applied, the sample height is allowed time to stabilise and is recorded as the consolidated height. Not only can the confined vertical stress-strain response be measured, but also the variation in bulk density during loading, provided the sample mass is known. During the loading process, the force acting on the top platen, as well as its displacement are recorded, from which the unconfined stress-strain curve can be obtained. The unconfined yield strength ($\sigma_u$) is the maximum vertical stress recorded during a test for a particular consolidation stress.

By repeating the experiment for a range of consolidation stresses the flow function of a bulk solid can be obtained quickly. In order to define the flow function, at least 3 data points are recorded for each stress level. If any value is more than 10% lower than the mean value, it is discarded. A minimum of 2 remaining points, after discarding the lowest value outside the 10% range, should then be used for the calculation of the average unconfined strength for a particular consolidation stress. Low values are discarded from the calculations as they can be caused by anomalies relating to the experimental procedure, such as, for example, non-uniform sample formation, alignment of a poorly formed sample or excessive disturbance of the sample while removing the confinement during a test. However all high values must be included in the reporting of the unconfined strength. In this study, four tests per consolidation stress have been recorded.

**Figure 1 – Edinburgh Powder Tester**

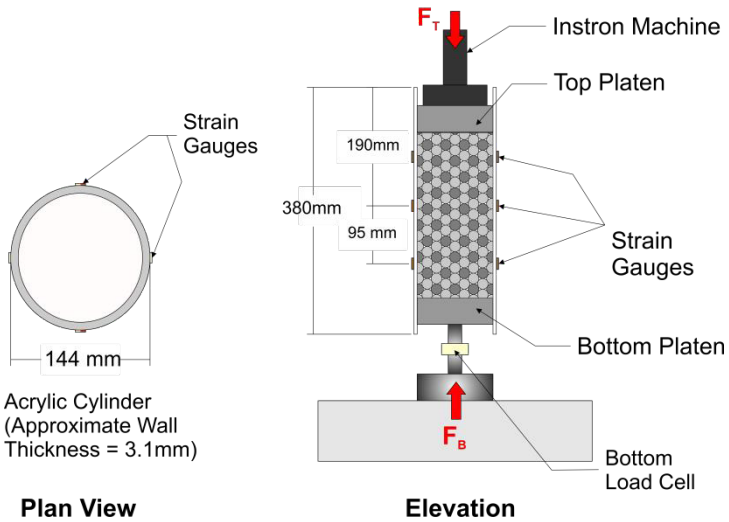


**Figure 2 – Confined Compression Tester**

### 2.3 Confined compression $K_o$ test

The response during confined compression of the iron ore fines was further observed by measuring the load transmitted laterally to the cylindrical walls from vertical loading in a separate confined compression tester (Fig. 2). In this tester, a load is applied to a granular material contained in the cylinder through a top platen driven by an Instron machine, at a constant displacement rate. A series of strain gauges are attached to the cylinder walls at several levels to allow precise measurement of the horizontal and vertical strains. Using membrane theory for thin walled vessels the stresses in the cylinder walls, and thus the granular solid, can be determined. With the vertical forces also being measured at both the top and bottom platens, the horizontal to vertical stress ratio, termed the lateral pressure ratio $K$, can be evaluated for the iron ore fines [8], [9]. This apparatus is a modified version of the one proposed by Masroor et al. [10], which is similar to the lambda tester in Eurocode 1 (EN 1991-4, 2004) for measuring the lateral pressure ratio for silo design [11].

## 3 EXPERIMENTAL RESULTS AND DISCUSSION

Figure 3 shows the stress-strain curves during confined compression in the EPT for both the KPRS and KPBO fines at various moisture contents. The corresponding bulk density variation is shown in Figure 4. For both materials significant bulk plasticity is evident with the unloaded density almost identical to the consolidated density. Both materials also exhibit the same trend; increasing axial strain with increasing moisture content up to a certain moisture content, above which the strain begins to reduce with further increases in moisture content. For the KPRS fines a maximum strain of approximately 37% is measured at 3.5% moisture content while the KPBO fines show a maximum strain of approximately 41% at 2.6% moisture content. The addition of moisture to the iron ore fines leads to the development of looser initial packing density and hence the increased measured strain with increasing moisture content. The effect is much more significant for the KPBO fines with the addition of just 2% moisture content leading to a change in density of almost 800 kg/m$^3$ compared to just over 400 kg/m$^3$ for the KPRS fines at double the moisture content.

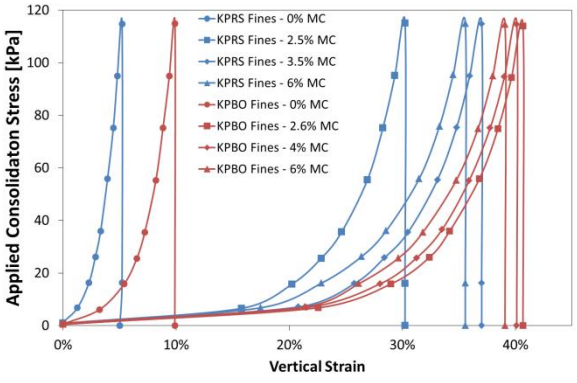


**Figure 3 – Stress-Strain during confined compression for both fines**

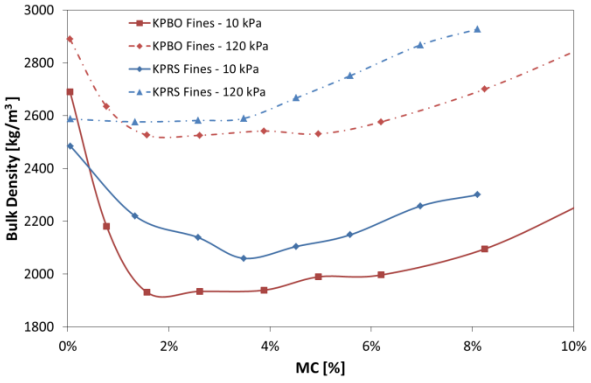


**Figure 4 - Bulk density during confined compression for both fines**

At moisture contents above 8% the KPRS fines form large agglomerates (greater than 10-15 mm) with significant irregular voids; as such the measurement of bulk density is no longer meaningful.

Figure 5 shows the unconfined stress-strain responses for KPRS at 20, 40, 60, 80 and 100 kPa consolidation stresses at a single moisture content (MC = 4%). All the curves show a hardening behaviour initially until peak failure occurs at the maximum unconfined strength; after that the curves descend, showing a softening behaviour. The unconfined strength increases with the consolidation stress.

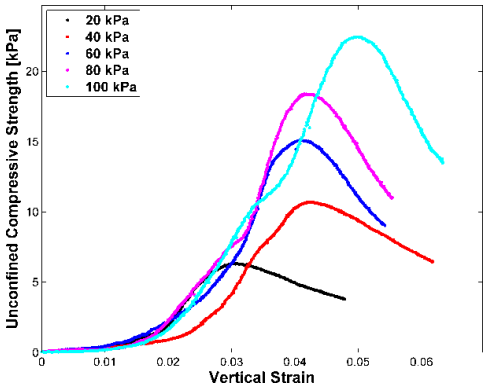


**Figure 5 - Stress-strain response for KPRS fines at 4% M.C.**

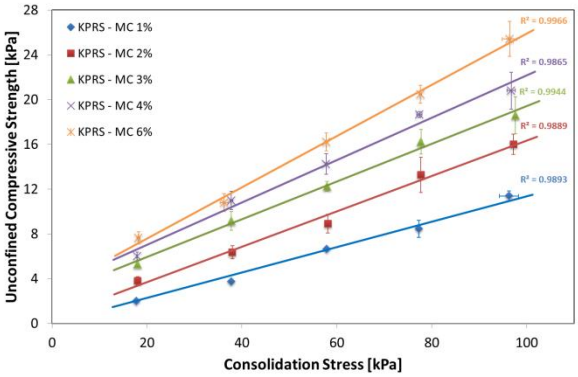


**Figure 6 - Flow function for KPRS fines**

From the unconfined tests, the flow function can be plotted as the best fit line through the test data. The flow functions for the two iron ore fines at different moisture levels are plotted in figure 6 and Figure 7 respectively.

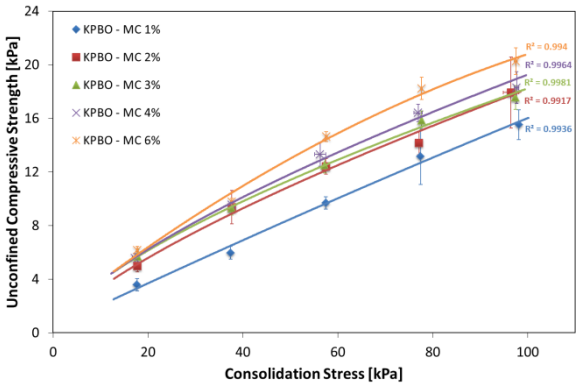


**Figure 7 - Flow function for KPBO fines**

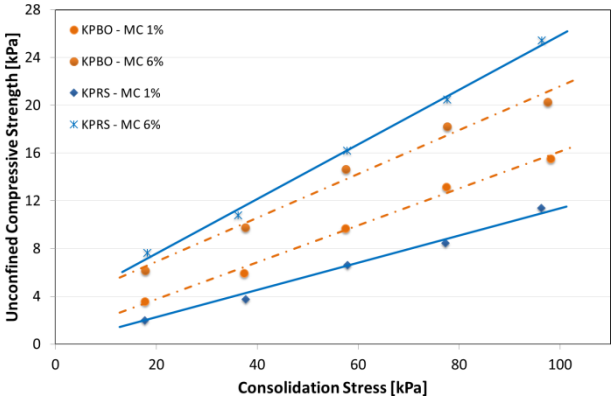


**Figure 8 - Flow function comparison**

A comparison of the range of flow function for the two type of fines is presented in Figure 8, where the highest and lowest values of both types of fines are included. From this it can be seen that the KPRS fines are more affected by increasing moisture content, with a greater increase in strength for the same increase in moisture content. While at low moisture contents the KPBO fines demonstrate a higher cohesion than KPRS, as the moisture content increases in the samples (≈ > 2%), the KPRS fines become more cohesive than the KPBO fines. This

suggests that KPRS fines will be more difficult to handle when a high moisture content is observed in the material.

Typical results from the confined compression tests are presented in Figure 9 with the stress strain and lateral pressure ratio evolution for dry KPBO fines plotted. As the stress level increases, the lateral pressure ratio *K* has been found to increase gradually and tend towards a constant value above approximately 20 kPa. For both types of dry fines this was observed to be approximately 0.24 with a slight increase observed as the moisture content was increased to approximately 6 %. Addition of further moisture above 6 % leads to a significant increase in the lateral pressure ratio for both types of fines. This is to be expected as the significant amounts of moisture act as a lubricant which can reduce the angle of internal friction leading to higher $K_0$ values. During unloading, the horizontal stress was increasingly "locked in" with the lateral pressure ratio increasing to an average value of ~0.6 at a vertical stress of 5 kPa. The results for both types of fines at various moisture contents are shown in Table 1 and the tests have been found to be consistent and repeatable with a coefficient of variation typically much less than 10% noted.

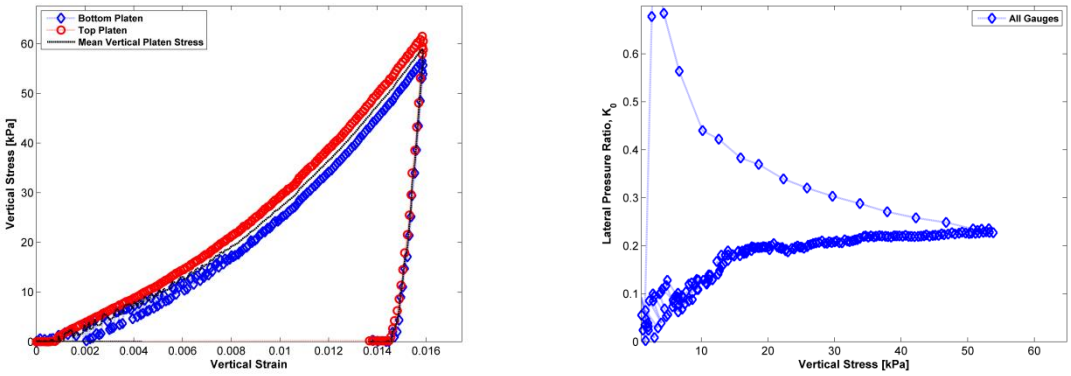


(a) Stress-strain response (b) Lateral pressure ratio evolution

**Figure 9 – Typical confined compression tests result for dry KPBO fines**

**Table 1 - Confined compresison test results for various types of fines**

| | KPBO Fines | | | KPRS Fines | | |
|---|---|---|---|---|---|---|
| **MC [%]** | 0.20 | 5.66 | 7.91 | 0.20% | 5.68 | 8.63 |
| **Peak Strain** | 0.016 | 0.096 | 0.078 | 0.018 | 0.106 | 0.077 |
| **$K_0$** | 0.235 | 0.246 | 0.293 | 0.241 | 0.254 | 0.302 |
| **Stress [kPa]** | 53.4 | 51.6 | 50.4 | 53.2 | 51.6 | 49.8 |

## 4 DEM IMPLEMENTATION

A DEM contact model based on an elasto-plastic model with adhesion [12], [13], [14] which implements hysteretic linear and non-linear loading paths [15] is deployed. The DEM contact model is based on the physical phenomena observed in AFM adhesive contact experiments [16]. When two particles or agglomerates are pressed together, they undergo elastic and plastic deformations and the pull-off (adhesive) force increases with an increase of the plastic contact area.

### 4.1 Contact Model

A non-linear contact model that accounts for both the elastic-plastic contact deformation and the contact-area dependent adhesion is presented. The schematic diagram of particle contact and normal force-overlap ($f_n$- $\delta$) for this model is shown in Figure 10 and may be mathematically expressed by equation (1).

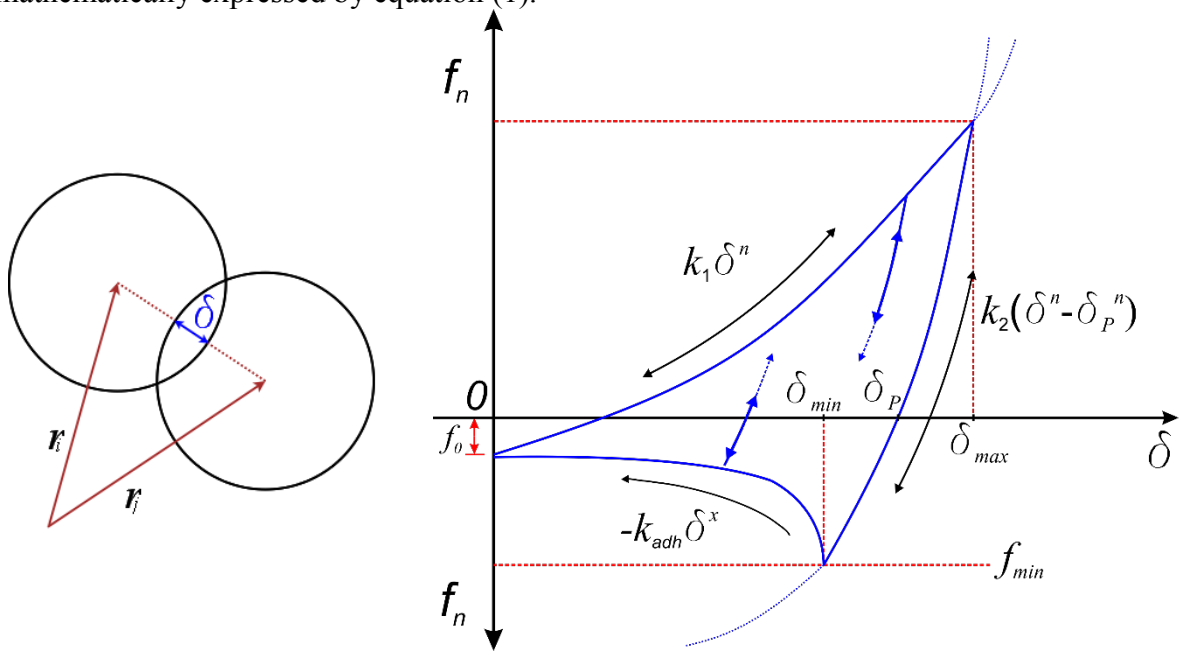


**Figure 10 - Normal Force-Overlap Relationship for Elasto-Plastic Adhesive Contact model**

In addition to the above-mentioned properties, a constant attractive force $f_0$ that can be used to account for the effect of van der Waals type forces is considered. The loading, unloading and re-loading, and adhesive branches are characterised by six parameters: the virgin loading stiffness parameter $k_1$, the unloading and reloading stiffness parameter $k_2$, the constant adhesion force $f_0$, the stiffness exponent $n$, the adhesion path exponent $X$ and the contact surface energy $\Delta\gamma$. The shape of all the three branches is controlled by the parameters $n$ and $X$ – they all become linear at an exponent value of unity [17], [18]. Furthermore, if $k_1$ is set equal to $k_2$ the model is reduced to an elastic contact model.

$$f_{hys} = \begin{cases} f_0 + k_1\delta^n & if\ k_2\left(\delta^n - \delta_p^n\right) \geq k_1\delta^n \quad (a) \\ f_0 + k_2\left(\delta^n - \delta_p^n\right) & if\ k_1\delta^n > k_2\left(\delta^n - \delta_p^n\right) > -k_{adh}\delta^x \quad (b) \\ f_0 - k_{adh}\delta^x & if\ -k_{adh}\delta^x \geq k_2\left(\delta^n - \delta_p^n\right) \quad (c) \end{cases} \tag{1}$$

During reloading, the contact force initially follows the unloading/reloading path $k_2$ but switches to the virgin loading path $k_1$ when the previous maximum loading force is reached. Unloading below the plastic overlap $\delta_p$ results in the development of an attractive force until the maximum attractive force $f_{min}$ is reached at $\delta_{min}$. Further unloading past this point results in a reduction in both the normal overlap and the attractive force until separation occurs. In this

study a value of $n$=1.5 has been used. The tangential force is calculated using the Mindlin tangential contact model. The rolling friction model is model A as defined by Ai et al. [19].

## 4.2 DEM Model Setup

A DEM model of equal dimensions to the EPT was created in the EDEM code [20], [21] to replicate the experimental setup. While the dimensions of the test setup are maintained, 10,000 paired particles with an aspect ratio of 1.5 were selected as the meso-scopic representation of the agglomerated real particles. Four different adhesion energy values have been selected to represent four different experimental moisture contents of 1%, 2%, 4% and 6%. The full set of parameters used for the simulations are given in Table 2. A simulation time-step of 2.5E-06, which is approximately $0.1\sqrt{m/k}$ has been selected for all simulations. Data is recorded for each simulation at a rate of 1000 Hz.

**Table 2 - Simulation Parameters**

| | | | |
|---|---|---|---|
| Particle Radius, R (m) | 0.00085 | Poisson's Ratio, ν | 0.225 |
| Particle Aspect Ratio, $AR_p$ | 1.5 | Adhesion Energy, Δγ ($J/m^2$) | 8,12.5,18.5,23.5 |
| Particle Density, ρ ($kg/m^3$) | 4150 | Particle Sliding Friction, $\mu_s$ | 0.5 |
| Young's Modulus, E (Pa) | 6.13E+06 | Particle Rolling Friction, $\mu_r$ | 0.005 |
| Shear Modulus, G (Pa) | 2.5E+06 | Wall Friction, $\mu_w$ | 0.0 |
| Spring Stiffness, $k_1$ (N/m) | 1.0E+05 | Platen Friction, $\mu_p$ | 0.5 |
| Spring Stiffness, $k_2$ (N/m) | 4.0E+06 | Simulation Time step (s) | 2.5E-06 |

The initial filling height varied with the DEM input parameters since increasing levels of particle adhesion lead to an increasingly looser initial packing. The consolidated aspect ratio of the sample for the DEM simulations was kept in a narrow range of 1.2 to 1.4 to reflect what was used in the experiment. Each simulation consists of three stages – filling the cylindrical mould to form the initial packing used for all stress levels; confined consolidation to the required stress level and subsequent unloading; and finally unconfined compression of the sample to failure after the removal of the mould. The process is visualised in Figure 11.

A random rainfall method was adopted to form a random packing as it represents a similar method employed during the experiments. Adhesion between the particles was accounted for in the filling process to allow for the development of a filled packing similar to the experiment. Following the particle generation all simulations were allowed a rest period to allow particles to settle and ensure that the systems were in a quasi-static state before the commencement of loading. Loading only commenced when the kinetic energy in the system reached a constant value that was less than $10^{-5}$ J. This ensured that particle velocities were in the region of $10^{-8}$ m/s with a constant coordination number. The confined consolidation process was conducted by translating the top platen vertically downwards at a constant rate of 25 mm/s (strain rate ≈ 0.3 $s^{-1}$) to apply a vertical compression. The process is similar to the procedure in the experiments.

After consolidating the sample to the desired stress level, the assembly was unloaded by translating the top platen upwards at the same constant speed. The lateral confining walls were removed when the unloading was complete and the unconfined sample was allowed to relax for a short period of time. This allowed the kinetic energy generated from the removal of the

confining wall and upward movement of the top platen to dissipate and drop to an acceptable stable value.

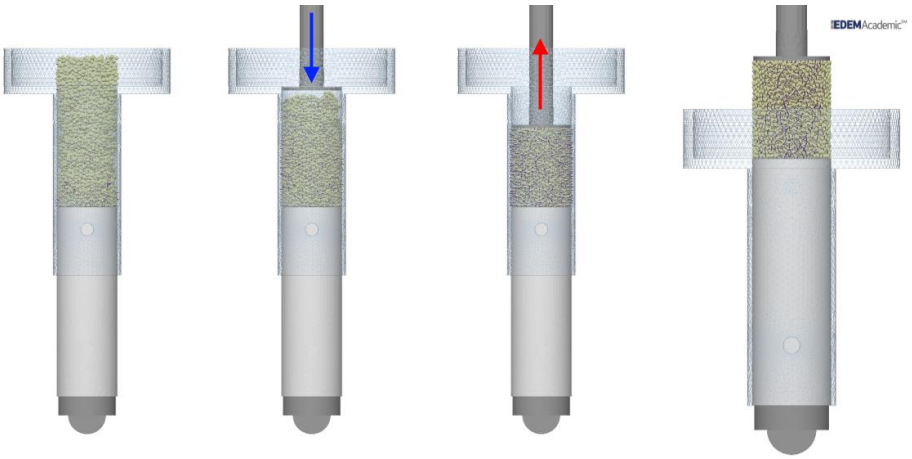


**Figure 11 - DEM simulation process**

The sample was then crushed to failure by moving the top platen downwards again at a constant rate of 5 mm/s (strain rate ≈0.05 $s^{-1}$). A higher compression rate was used for the confined compression as the inertial effect of the higher loading rate is not as significant as in the unconfined compression test, where a high platen velocity can lead to impact damage of the sample at the point of initial loading in the unconfined test. In all tests the bottom platen, which represents the stationary base in the experiments remained stationary in all stages.

## 5 DEM SIMULATION RESULTS

A comparison between the predicted DEM bulk densities and the experimentally recorded values is made in Figure 12. There is strong agreement between the DEM simulations at the higher stresses of 60 and 100 kPa. A larger scatter is observed at 20 kPa. In all cases the DEM simulation with the lowest adhesion energy lead to the densest packing. In almost all cases the DEM result is within the experimental scatter for the corresponding experimental result.

The peak unconfined yield strength is plotted against the consolidation stress to provide the flow function in Figure 13 with the corresponding experimental result also included for comparison. A linear best fit line through the DEM simulation results was found for all adhesion energies.

The DEM results show a strong dependence on the prior consolidation stress applied and are in close agreement with those obtained experimentally from the EPT. Both display a similar linear trend with increasing adhesion. Increasing unconfined strength with increasing levels of adhesion is also found to be similar to the experiment where the increasing moisture content led to an increased unconfined strength. In many cases the DEM simulation result lies within the standard deviations found in the EPT tests.

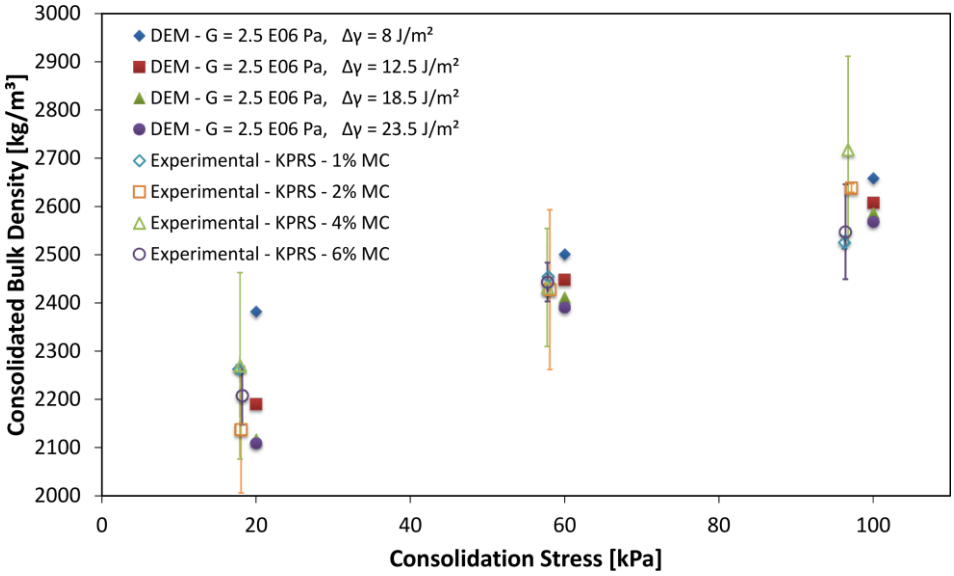


**Figure 12 - Bulk Density comparison**

At lower moisture contents the DEM simulation results are in close agreement with the experiment for higher consolidation stresses but over-predicts the unconfined strength below a consolidations stress of 60 kPa. A better match is found between the higher moisture content experimental results and the higher adhesion energy DEM simulations, with both producing similar values of unconfined strength across all consolidation stresses.

In all these simulations, only the adhesion energy parameter has been modified and this has been shown to be an excellent approximation of the addition of moisture content to the iron ore fines and is able to replicate the experimental flow function.

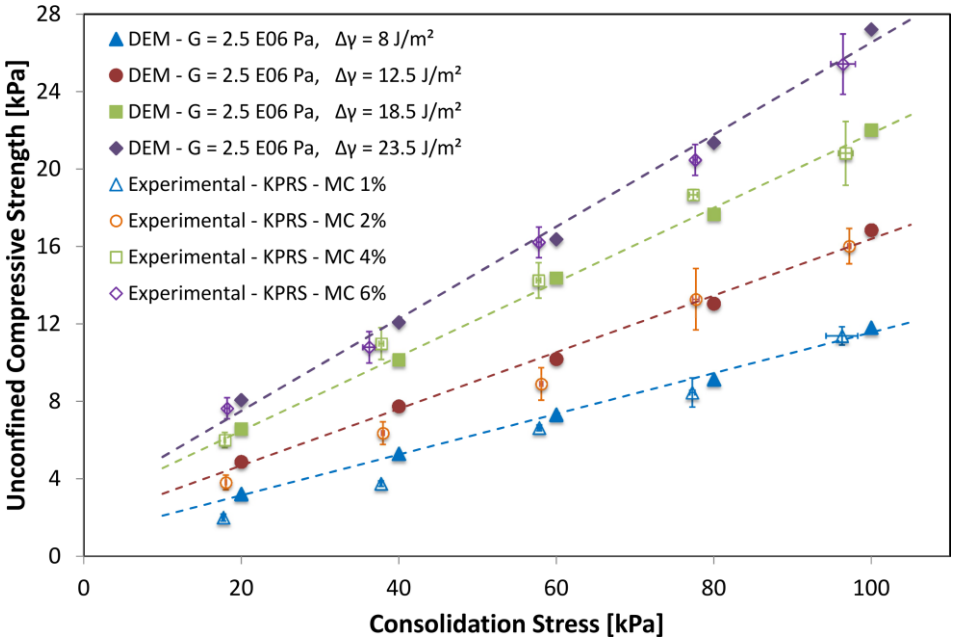


**Figure 13 - Flow-function comparison for simulation and experiments for KPRS fines**

## 6 CONCLUSIONS

The effect of moisture content on the behaviour of the iron ore fines has been evaluated and both types of fines have shown a significant dependence on the moisture content for the development of cohesion to occur. A significant difference in the response of both materials in both confined and unconfined compression has also been observed. KPRS fines have a much higher unconfined strength and flow function at higher moisture contents, and also show a greater increase in cohesion with the addition of moisture. This suggests more difficult handling for KPRS fines in wetter conditions.

The lateral pressure ratio for both iron ore fines has been evaluated from a confined compression test and a similar value of the order of 0.25 was noted for each type of fines at various moisture content. The lateral pressure ratio was found to increase slightly between 0% to 6% moisture content, with a significant increase noted above 6% moisture content, rising to approximately 0.3.

DEM simulations have been carried out to replicate the EPT experiment on KPRS fines for various moisture contents using the elasto-plastic adhesive model. The results show an excellent agreement between the DEM simulation and experimental result across a range of consolidation stresses and adhesion levels. The results also show the ability of the contact model to capture the stress history dependent behaviour of a cohesive granular solid across a range of adhesion levels.

## REFERENCES

[1] K. L. Johnson, K. Kendall, and A. D. Roberts, "Surface Energy and the Contact of Elastic Solids," *Proceedings of the Royal Society A: Mathematical, Physical and Engineering Sciences*, vol. 324, no. 1558, pp. 301–313, Sep. 1971.

[2] G. Lian, C. Thornton, and M. J. Adams, "A theoretical study of the liquid bridge forces between two rigid spherical bodies," *Journal of Colloid and Interface Science*, no. 161, pp. 138–147, 1993.

[3] T. Mikami, H. Kamiya, and M. Horio, "Numerical simulation of cohesive powder behavior in a fluidized bed," *Chemical Engineering Science*, vol. 53, no. 10, pp. 1927–1940, May 1998.

[4] T. Gröger, U. Tüzün, and D. M. Heyes, "Modelling and measuring of cohesion in wet granular materials," *Powder Technology*, vol. 133, no. 1–3, pp. 203–215, Jul. 2003.

[5] B. Remy, J. G. Khinast, and B. J. Glasser, "Wet granular flows in a bladed mixer: Experiments and simulations of monodisperse spheres," *AIChE Journal*, vol. 58, no. 11, 2012.

[6] J. P. Morrissey, S. C. Thakur, J. Sun, J. F. Chen, and J. Y. Ooi, "Modelling Cohesive-Frictional Particulate Solids For Bulk Handling Applications," in *II International Conference on Particle-based Methods – Fundamentals and Applications - PARTICLES 2011*, 2011, pp. 1–11.

[7] S. C. Thakur, J. P. Morrissey, J. Sun, J. F. Chen, and J. Y. Ooi, "A DEM study of cohesive particulate solids : plasticity and stress- history dependency," 2011, pp. 1–5.

[8] Y. C. Chung and J. Y. Ooi, "Confined compression and rod penetration of a dense granular medium : discrete element modelling and validation," *Modern Trends in Geomechanics*, pp. 223–239, 2006.

[9] Y. C. Chung and J. Y. Ooi, "Influence of Discrete Element Model Parameters on Bulk Behavior of a Granular Solid under Confined Compression," *Particulate Science and Technology*, vol. 26, no. 1, pp. 83–96, Dec. 2007.

[10] S. A. Masroor, L. W. Zachary, and R. A. Lohnes, "A test apparatus for determining elastic constants of bulk solids," in *SEM Spring Conference on Experimental Mechanics*, 1987, pp. 46–63.

[11] British Standards Institution, *BS EN 1991-4:2006: Eurocode 1 — Actions on structures — Part 4: Silos and tanks*, vol. 3, no. July. British Standards Institution, London, UK., 2006, pp. 1–112.

[12] S. Luding, "Introduction to discrete element methods," *European Journal of Environmental and Civil Engineering*, vol. 12, no. 7–8, pp. 785–826, Aug. 2008.

[13] J. Tomas, "Adhesion of ultrafine particles—A micromechanical approach," *Chemical Engineering Science*, vol. 62, no. 7, pp. 1997–2010, Apr. 2007.

[14] O. R. Walton and R. L. Braun, "Viscosity, granular-temperature, and stress calculations for shearing assemblies of inelastic, frictional disks," *Journal of Rheology*, vol. 30, no. 5, pp. 949–980, 1986.

[15] J. P. Morrissey, "Discrete Element Modelling of iron ore fines to include the effects of moisture and fines," University of Edinburgh, 2013.

[16] R. Jones, "From Single Particle AFM Studies of Adhesion and Friction to Bulk Flow: Forging the Links," *Granular Matter*, vol. 4, no. 4, pp. 191–204, Feb. 2003.

[17] S. Luding, "Cohesive, frictional powders: contact models for tension," *Granular Matter*, vol. 10, no. 4, pp. 235–246, Mar. 2008.

[18] S. Luding, "Anisotropy in cohesive, frictional granular media," *Journal of Physics: Condensed Matter*, vol. 17, no. 24, pp. S2623–S2640, Jun. 2005.

[19] J. Ai, J. F. Chen, J. M. Rotter, and J. Y. Ooi, "Assessment of rolling resistance models in discrete element simulations," *Powder Technology*, vol. 206, no. 3, pp. 269–282, Jan. 2011.

[20] DEM Solutions Ltd., *EDEM 2.4.3 User Guide*. Edinburgh, UK, 2012.

[21] DEM Solutions Ltd., *EDEM 2.3 User Guide*, Revision 2. Edinburgh, UK: DEM Solutions Ltd., 2010, pp. 1–139.